ELSEVIER

International Journal of Heat and Fluid Flow 21 (2000) 389–402

International Journal of HEAT AND FLUID FLOW

www.elsevier.com/locate/ijhff

Statistical simulation of particle deposition on the wall from turbulent dispersed pipe flow

Edgar Akio Matida *, Koichi Nishino, Kahoru Torii

Department of Mechanical Engineering and Materials Science, Yokohama National University, 79-5 Tokiwadai, Hodogaya-ku, Yokohama 240-8501, Japan

Received 9 February 1999; accepted 26 November 1999

Abstract

Deposition of particles towards the wall from a turbulent dispersed flow in a vertical pipe has been studied numerically. A fully developed turbulent pipe flow of air is chosen as the primary flow, and it is represented by the law-of-the-wall relations and the average turbulence statistics obtained from a direct numerical simulation reported in the literature. Trajectories and velocities of the particles are calculated, using a one-way coupling Lagrangian eddy–particle interaction model. Thousands of individual particles (typically 920 kg/m^3 in density) of various diameters (2.0–68.5 μm) are released in the represented flow, and deposition velocities are evaluated. It is shown that the deposition velocities predicted are in good agreement with experimental data available in the literature. The influence of some forces in the particle equation of motion (i.e., the Saffman lift force, the centrifugal force, the conservation of angular momentum and the buoyancy force) on the prediction of the deposition velocities is examined. Also examined is the influence of the inlet particle concentration profile, on which little attention has been paid so far. The unique phenomenon of 'near-wall build-up' of small particles, which has been reported in some previous simulations and experiments, was also observed in the present simulation while the result for very small particles ($\tau_p^+ < 3$) should be accepted with reservation due to their possible spurious build-up associated with the random-walk approach.

Keywords: Two-phase flow; Turbulent pipe flow; Particle deposition; Numerical simulation; Lagrangian particle tracking; One-way coupling

1. Introduction

The deposition of solid or liquid particles from a turbulent flow onto the adjacent walls is observed in many industrial applications, for example, nuclear reactor systems, gas turbine blades, oil-conveyance pipe lines, cyclone separators, spray cooling, painting and sandblasting. The situation in some of these applications can be simplified as the deposition from a turbulent dispersed pipe flow, which can be regarded as a good starting point for studying this complex two-phase flow phenomenon.

McCoy and Hanratty (1977) compiled experimental data of deposition rates onto the vertical pipe wall measured by several authors for liquid and solid particles, ranging from sub-microns to hundred of microns in diameter (refer to Fig. 1). They plotted the dimensionless deposition velocities, k_p/u^*, as a function of the dimensionless particle relaxation time, τ_p^+, which is defined as

$$\tau_p^+ = S^+ \frac{u^*}{U_{p0}} = \frac{d_p^2 \rho_p U_{p0} u^*}{18 \mu_f \nu_f} \frac{u^*}{U_{p0}} = \frac{d_p^2 \rho_f^2 u^{*2}}{18 \mu_f^2} \frac{\rho_p}{\rho_f}, \quad (1)$$

where S^+ is the dimensionless stopping distance. Stopping distance is the distance a particle would travel through a stagnant fluid with an initial velocity, U_{p0}, under the conditions of Stokesian drag. The particle deposition velocity is defined as $k_p = m_p/\bar{C}$, where m_p is the rate of deposition of particle (i.e., mass flux) and $\bar{C}$ is the bulk mean particle concentration (i.e., mass of particles loaded in unit flow volume). McCoy and Hanratty proposed the piecewise best fittings for the experimental data as shown in Fig. 1. In the sub-micron range ($\tau_p^+ < 0.15$), particles follow the fluid motions and the Brownian diffusion is the mechanism responsible for the deposition, suggesting that k_p/u^* is independent of τ_p^+. In the range of $0.2 < \tau_p^+ < 22.9$, the best fit of all compiled data is represented by $k_p/u^* = 3.25 \times 10^{-4}(\tau_p^+)^2$, while the best fit for $\tau_p^+ > 22.9$ is given by $k_p/u^* = 0.17$. For $\tau_p^+ > 15,000$, McCoy and Hanratty proposed that k_p/u^* is inversely proportional to the particle diameter as $k_p/u^* = 20.7(\tau_p^+)^{-0.5}$.

The prediction of the rate of deposition of particles is an important issue and usually handled by two approaches. The first approach is Eulerian, where particles are assumed to move

* Corresponding author: Tel.: +81-45-339-3895; fax: +81-45-339-3901.

E-mail address: machi@tori.me.ynu.ac.jp (E.A. Matida).

0142-727X/00/$ - see front matter
PII: S0142-727X(00)00004-7

Notation

A	cross-sectional area, m^2
C	mass concentration, kg/m^3
C_1	coefficient for eddy lifetime
C_μ	coefficient in k–ε turbulence model
d	diameter, m
F	fraction of particles that reach the sampling cross-section
g	gravitational acceleration, m/s^2
H	wall-to-wall channel height, m
J_u	factor defined by McLaughlin (1991)
k	turbulence kinetic energy, m^2/s^2
k_p	particle deposition velocity, m/s
L_e	length scale of fluid eddy, m
M	mass flow rate, kg/s
m	mass flux, $kg/s/m^2$
N	number
r	radius, m
Re	Reynolds number of pipe flow ($=U_m d_t/\nu_f$)
Re_p	particle Reynolds number ($=U_r d_p/\nu_f$)
S	stopping distance, m
t	time, s
U	velocity, m/s
U_r	relative velocity ($=[(u_f-u_p)^2+(v_f-v_p)^2+(w_f-w_p)^2]^{0.5}$), m/s
U_m	bulk mean velocity, m/s
u^*	friction velocity, m/s
u, v, w	axial, radial and azimuthal velocities, m/s
y	distance from the wall, m
x	axial distance, m

Greeks

α	coefficient for Reynolds number effect on viscous drag, s
β	ratio of Lagrangian timescale to Eulerian timescale
Δt	time step for numerical integration, s
ε	dissipation rate of turbulence kinetic energy, m^2/s^3
ε_M	parameter according to McLaughlin (1991)
λ	Taylor microscale, m
μ	dynamic viscosity, N s/m^2
ν	kinematic viscosity, m^2/s
ρ	density, kg/m^3
τ_e	lifetime of fluid eddy, s
τ_p	relaxation time of particle, s
χ	volume fraction

Subscripts

E	Eulerian
e	eddy
f	fluid
L	Lagrangian
p	particle
rms	root-mean-square (RMS) value
s	sampling
t	pipe
0	initial value

Superscripts

$\overline{(\,)}$	average
$(\,)'$	fluctuation
$(\,)^+$	non-dimensionalization by wall variables (u^* and ν_f)

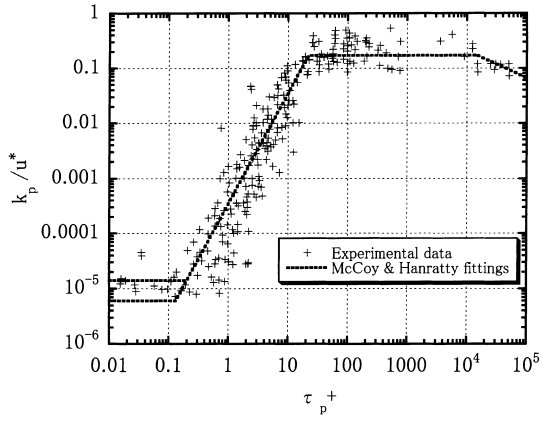

Fig. 1. Experimental data for dimensionless particle deposition velocities (McCoy and Hanratty 1977).

toward the adjacent wall by turbulent diffusion and then reach the wall by a free flight mechanism (see Friedlander and Johnstone, 1951; Beal, 1970; Ganic and Mastanaiah, 1981; Lee and Wiesler, 1987; Yang and Lee, 1991). The second approach is Lagrangian, where trajectories of individual particles are calculated by solving the particle equation of motion. The Lagrangian approach has a computational expense which is higher than the Eulerian approach, but it is capable of providing a more realistic and flexible model of particle deposition than the Eulerian one. When the particle concentration is very low, the primary flow is assumed to be unmodified by the presence of particles (i.e., one-way coupling), the assumption which significantly facilitates simulations of particle motions. On the other hand, when the particle concentration is not very low, the mutual interaction between the primary flow and the particles must be incorporated into the simulation (i.e., two-way coupling). The present study deals with the conditions of low particle concentration, and the one-way coupling approach is adopted in the simulation.

Eddy–particle interaction model is a Lagrangian approach used to track particles in the simulation of flows laden with particles. Given initial conditions of velocity and position, the motion of a single particle is calculated by treating it as a series of interactions with discrete eddies having a characteristic size, lifetime and velocity. Graham and James (1996) classified eddy interaction models that have appeared in the literature into the following three types. The first assumed that the characteristic eddy scales remained constant throughout the flow, e.g., Hutchinson et al. (1971). The second used the characteristic eddy scales defined by the primary flow, e.g., Gosman and Ioannides (1981), Govan et al. (1989) and Kallio and Reeks (1989). The third consisted of alternative models, in which, besides representative length scale, lifetime and velocity scale, other forms of Lagrangian or Eulerian velocity auto-correlation functions were required, e.g., Berlemont et al. (1990) and Burry and Bergeles (1993).

One-way coupling Lagrangian eddy–particle interaction models have been used to predict the rate of deposition of particles by, e.g., Kallio and Reeks (1989) and Govan et al. (1989). Their results are plotted in Fig. 2 and compared with the McCoy–Hanratty fittings. To represent the primary flow in a pipe, Kallio and Reeks (1989) used the law-of-the-wall profile for the mean velocity and an empirical function for the RMS values of wall-normal velocity fluctuations. They performed two-dimensional calculations only in the near-wall region ($y^+ < 200$) and did not include the terms representing

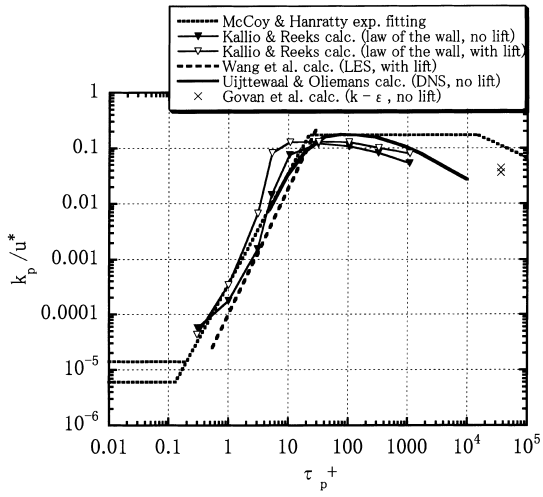

Fig. 2. Calculation results for dimensionless particle deposition velocities.

the centrifugal force and the conservation of angular momentum in the particle equation of motion. As shown later in this paper, those terms have an appreciable influence on the deposition of large, heavy particles in turbulent pipe flows. Govan et al. (1989) used conventional k–ε turbulence models to represent a fully developed turbulent pipe flow. Particle diameters ranging from 110 to 550 μm ($\tau_p^+ = 7,000 \sim 175,000$) were examined, but their method was not tested for $\tau_p^+ < 7,000$. When using conventional k–ε turbulence models, three-component velocity scales of fluid eddies are given by the isotropic decomposition of turbulence kinetic energy (i.e., $u'_{rms} = v'_{rms} = w'_{rms} = (2k/3)^{0.5}$). However, it is known that the actual RMS values of radial velocity fluctuations in the wall-bounded turbulent shear flows are substantially smaller near the wall than the values of isotropic decomposition of k. More recently, Uijttewaal and Oliemans (1996) and Wang et al. (1997) used large eddy simulation (LES) and direct numerical simulation (DNS) combined with the one-way coupling approach for the prediction of particle motions. They reported particle deposition velocities in good agreement with the McCoy–Hanratty fittings (refer to Fig. 2). Although these simulations can reproduce the primary flow in a most realistic manner, their high cost of computation limits themselves to the flows of low Reynolds number and simple flow geometry.

From a practical point of view, the use of Reynolds-averaged Navier–Stokes (RANS) equations, such as the k–ε turbulence model equations, is cost-effective and thus preferable for the prediction of the primary flow. As the RANS equations provide only one-point turbulence statistics, it is of great significance to demonstrate that, once correct turbulence statistics are given, the one-way coupling Lagrangian eddy–particle interaction model can predict adequately the particle deposition onto the walls. As shown later in this paper, an accurate prediction of particle deposition relies heavily on the sufficient resolution of near-wall turbulence statistics of the primary flow. Unfortunately, no available RANS equations at their current stage seem to have enough capability, even for canonical turbulent flows such as pipe flows and channel flows as far as the region very close to the wall is concerned. For this reason, the present study has adopted the primary flow representation established through careful curve fitting to the one-point turbulence statistics obtained by a recent direct numerical simulation of a turbulent channel flow. Obviously, the present approach *may not* be extended to more complex turbulent flows where no DNS or LES results are available. However, it is foreseen that a combined use of RANS equations with newly emerging experimental techniques such as particle image velocimetry will provide a way for predicting accurate near-wall turbulence statistics of the primary flow through careful optimization of parameters in the RANS equations.

The present work simulates three-dimensional motions of particles released in a vertical turbulent pipe flow. The influence of inlet particle concentration profile and length of the test section, to which little attention has been paid in previous experiments and simulations, are carefully examined here. Also examined is the effect of various forces, such as Saffman lift force, centrifugal force, conservation of angular momentum and gravitational force, on the prediction of the deposition velocities. The unique and experimentally verified phenomenon of 'near-wall build-up' is predicted for small particles (say $\tau_p^+ < 10$) in the present simulations. The result is compared with previous simulation results and discussed in relation to the spurious build-up known to become conspicuous for very small particles in the random-walk approach.

2. Lagrangian simulation

2.1. Primary flow representation

A proper representation of the primary flow is crucial for adequate prediction of the deposition rate of particles. In the course of the study, it is recognized that the rate of deposition of small particles is considerably overpredicted when a conventional k–ε turbulence model is used for the prediction of the primary flow. To have more accurate representation of the primary flow, the present simulation has adopted the axial mean velocity ($\bar{u}_f$) given by the law-of-the-wall equations and the RMS values of fluctuating velocities (u'_{rms}, v'_{rms} and w'_{rms}) curve-fitted to the DNS data of a two-dimensional channel flow of Mansour used by Dreeben and Pope (1997). The turbulence dissipation rate, ε, is also curve-fitted to the same DNS data. The fittings are summarized in Table 1 and compared with the DNS data in Fig. 3. The friction velocity for normalization is evaluated from Blasius' formula, $u^* = [0.03955Re^{-0.25}]^{0.5}U_m$. It is seen that the present curve fittings reproduce the DNS data faithfully in the entire region. Note that the fittings of u'_{rms} and w'_{rms} satisfy the accepted wall-asymptotic behaviors ($u'_{rms} \to 0.4y^+$ and $w'_{rms} \to 0.2y^+$), while the fitting of v'_{rms} gives slightly larger value than the accepted wall-limiting value ($v'_{rms} \to 0.009y^{+2}$).

The present representation of the primary flow mentioned above should be accurate only for turbulent channel and pipe flows of Reynolds numbers comparable to that of the DNS, $Re = U_m H/\nu_f = 13{,}000$. However, it is shown that the profile of v'_{rms} near the wall (say, $y^+ < 50$) is relatively insensitive to the change of Reynolds number (Antonia et al., 1992). Since the profile of v'_{rms} is most influential on the prediction of deposition rates, it is expected that the present representation be valid for a wide range of Reynolds numbers. In fact, the experimental results of Liu and Agarwal (1974) indicate that the deposition rates for different Reynolds numbers (10,000 and 50,000) are practically the same for $\tau_p^+ = 4 \sim 40$.

2.2. Particle equation of motion

Tchen extended the work of Basset, Boussinesq and Ossen and proposed an equation for the motion of a rigid sphere in a non-uniform flow (Hinze, 1975). Corrsin and Lumley (1956) modified Tchen's equation by including a term for turbulence pressure gradients. After rigorous analysis, Maxey and Riley (1983) proposed an equation of motion of a small sphere with

Table 1
Pipe flow representation

Direction	Mean velocities	RMS values of fluctuating velocities
Axial	$y^+ < 5: \ \bar{u}_f^+ = y^+$ $5 < y^+ < 30: \ \bar{u}_f^+ = -3.05 + 5\ln y^+$ $y^+ > 30: \ \bar{u}_f^+ = 2.5\ln y^+ + 5.5$	$\frac{u'_{\rm rms}}{u^*} = \frac{0.40y^+}{1 + 0.0239(y^+)^{1.496}}$.
Radial	$\bar{v}_{\rm f} = 0$	$\frac{v'_{\rm rms}}{u^*} = \frac{0.0116(y^+)^2}{1 + 0.203y^+ + 0.00140(y^+)^{2.421}}$.
Azimuthal	$\bar{w}_{\rm f} = 0$	$\frac{w'_{\rm rms}}{u^*} = \frac{0.19y^+}{1 + 0.0361(y^+)^{1.322}}$
	$\varepsilon^+ = \frac{1}{4.529 + 0.0116(y^+)^{1.75} + 0.768(y^+)^{0.5}}$	

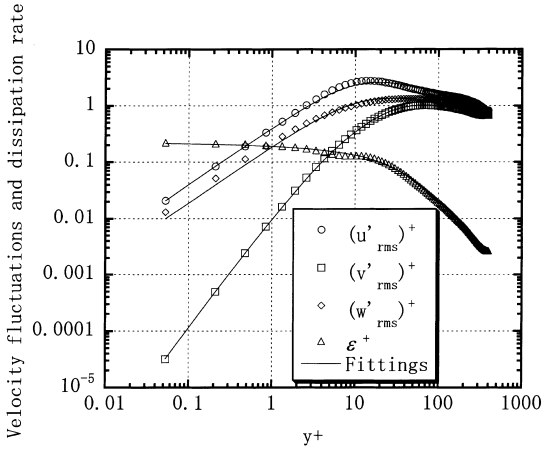

Fig. 3. Comparison between the present curve fittings and the DNS data.

relative motion of low Reynolds number. More recently, Mei (1996) proposed an equation of particle motion applicable to finite Reynolds number.

Considering relatively small particles with low density ratios, $\rho_{\rm f}/\rho_{\rm p} \ll 1$, and taking into account only viscous drag, gravity and corrected Saffman lift force (Saffman, 1965; McLaughlin, 1991), the following three-dimensional Lagrangian equations that describe the movement of a particle in the cylindrical coordinate system were adopted in the present simulation:

$$\frac{{\rm d}u_{\rm p}}{{\rm d}t} = \frac{(u_{\rm f} - u_{\rm p})}{\tau_{\rm p}/\alpha} - g\left(1 - \frac{\rho_{\rm f}}{\rho_{\rm p}}\right)$$

$$\frac{{\rm d}v_{\rm p}}{{\rm d}t} = \frac{(v_{\rm f} - v_{\rm p})}{\tau_{\rm p}/\alpha} + \frac{w_{\rm p}^2}{r_{\rm p}} + \frac{54\mu_{\rm f}}{4\pi^2 d_{\rm p}\rho_{\rm p}} J_u \,{\rm sgn}\left(\frac{\partial u_{\rm f}}{\partial y}\right)\left(\frac{1}{v_{\rm f}}\left|\frac{\partial u_{\rm f}}{\partial y}\right|\right)^{1/2}(u_{\rm f} - u_{\rm p}), \qquad (2)$$

$$\frac{{\rm d}w_{\rm p}}{{\rm d}t} = \frac{(w_{\rm f} - w_{\rm p})}{\tau_{\rm p}/\alpha} - \frac{w_{\rm p}v_{\rm p}}{r_{\rm p}},$$

where

$$\alpha = 1 + 0.15Re_{\rm p}^{0.687}. \qquad (3)$$

Note that the velocities in Eq. (2) are instantaneous quantities composed of the mean part and the fluctuating part as, e.g., $u_{\rm f} = \bar{u}_{\rm f} + u'_{\rm f}$. The terms representing the centrifugal force, $w_{\rm p}^2/r_{\rm p}$, and the conservation of angular momentum, $-w_{\rm p}v_{\rm p}/r_{\rm p}$, appear in the equations for $v_{\rm p}$ and $w_{\rm p}$, respectively. Also note that the above particle equations of motion may not be valid for very small particles ($\tau_{\rm p}^+ < 0.1$) because of the absence of random force terms responsible for Brownian motions of particles.

Particle trajectories are calculated by integrating twice the above equations using fourth-order Runge–Kutta method. The gradient of instantaneous fluid velocity in the lift force in the equation for $v_{\rm p}$ is replaced by $\partial\bar{u}_{\rm f}/\partial y$ at a location of the particle. $J_{\rm u}$ is the factor proposed by McLaughlin (1991), which corrects the Saffman lift force in the situations where the slip velocity between the particle and the primary flow is large. $J_{\rm u}$ is given as follows:

$$\varepsilon_{\rm M} = \frac{{\rm sgn}\left(\frac{\partial u_{\rm f}}{\partial y}\right)\left(\frac{1}{v_{\rm f}}\left|\frac{\partial u_{\rm f}}{\partial y}\right|\right)^{1/2}}{(u_{\rm p} - u_{\rm f})}, \qquad (4)$$

where $\partial\bar{u}_{\rm f}/\partial y$ is used again to evaluate the gradient of instantaneous fluid velocity in the above equation. For $0.025 \leqslant |\varepsilon_{\rm M}| \leqslant 20$, $J_{\rm u}$ is interpolated linearly from tabulated values given by McLaughlin (1991, Table 1 in his paper) and for large and small $\varepsilon_{\rm M}$, the following equations proposed by McLaughlin are used:

$$J_{\rm u} = 2.255 - 0.6463/\varepsilon_{\rm M}^2 \quad \text{for } |\varepsilon_{\rm M}| \gg 0, \qquad (5)$$

$$J_{\rm u} = -32\pi^2|\varepsilon_{\rm M}|^5 \ln(1/\varepsilon_M^2) \quad \text{for } |\varepsilon_{\rm M}| \ll 0. \qquad (6)$$

On the basis of the results given by McLaughlin (1993), Chen and McLaughlin (1995) extended the approach of McLaughlin (1991) by proposing the use of three different equations for the lift force depending on the particle position from the wall. They showed that the lift force acting on a particle near the wall (say, $y^+ < 2$) could be positive (away from the wall) even when the particle led the fluid, implying a reduced significance of the lift force on the rate of particle deposition. Their approach was further modified by Wang et al. (1997), who performed LES of turbulent channel flow and reported that the lift force actually imposed very little influence on the rate of deposition of very small particles ($\tau_{\rm p}^+ < 2$) but had a substantial influence on the rate of deposition of larger particles. Although the approach of Wang et al. is based on firm physical considerations, their expression of the lift force very near the wall gives values appreciably lower than the recent experimental results by Mollinger and Nieuwstadt (1996).

Considering such unresolved discrepancies as well as the complexity of the approach of Wang et al. (1997), the present simulation has employed the approach of McLaughlin (1991) for the evaluation of the lift force. It must be addressed here that a small difference that might be caused by the choice of approach for lift force can be obscured by the present simplification of the replacement of instantaneous velocity gradient with the local mean velocity gradient, and therefore that the employment of a more elaborate approach such as that of Wang et al. needs to be accompanied by a proper evaluation of instantaneous velocity gradient within the framework of RANS equations.

2.3. Eddy–particle interaction model

The eddy–particle interaction model is illustrated in Fig. 4. At the start of a particular eddy–particle interaction, the particle with initial velocity, u_{p0}, is located at the center of an eddy with a velocity scale, u_e, which remains constant during the interaction. The eddy translates with the instantaneous fluid velocity, but the particle will have another trajectory according to its equation of motion. A new interaction starts when the eddy lifetime is over or the particle crosses the eddy (i.e., the distance between the center of the eddy and the center of the particle exceeds the length scale of the eddy).

On the basis of the method of Gosman and Ioannides (1981), Schuen et al. (1983) simulated the particle dispersion in a turbulent round jet, where they used a k–ε turbulence model along with the following characteristic scales of fluid eddies:

$$L_e = (C_\mu)^{3/4}\frac{k^{3/2}}{\varepsilon}, \quad \tau_e = \frac{L_e}{(2k/3)^{0.5}} \quad \text{and} \quad u_e = \sqrt{\frac{2}{3}k}. \tag{7}$$

Graham and James (1996) noted that k–ε models using these scales for non-homogeneous turbulence underestimate particle dispersion and suggested that the lifetime and the length scale should have the values doubled.

Considering that the Lagrangian timescale is proportional to the Eulerian integral timescales in homogeneous isotropic stationary turbulence, Kallio and Reeks (1989) have estimated the Lagrangian integral timescale by

$$\tau_L = \beta\tau_E \cong 0.8\beta\frac{k}{\varepsilon}. \tag{8}$$

Here, β is a function of the turbulent Reynolds number ($Re_\lambda = u'\lambda/v$), varying from 0.6 to 0.3 for $Re_\lambda = 20$ to 70, according to Sato and Yamamoto's (1987) measurements. Hinze (1975, p. 426) has proposed β being approximately 0.4. The Lagrangian timescale is the longest time interval that a particle will continue moving in the same direction. It is thus assumed here that in the case of simulating particle deposition onto the wall from an internal pipe flow the use of the variance of radial (or wall-normal) velocity fluctuations is appropriate for modeling τ_L as follows:

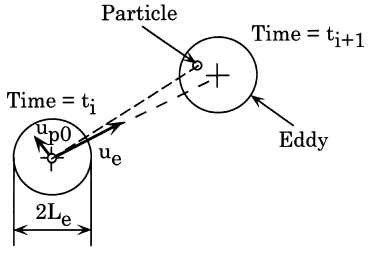

Fig. 4. Eddy–particle interaction model.

$$\tau_L \cong C_1\frac{(v'_{rms})^2}{2\varepsilon}. \tag{9}$$

As $k \cong 3.5(v'^2_{rms}/2)$ in the core region of the pipe flow, τ_L is given as

$$\tau_L \sim (0.42\text{–}0.84)\frac{(v'_{rms})^2}{\varepsilon}. \tag{10}$$

In the report of Kallio and Reeks (1989), in order to give self-consistent dispersion properties in homogeneous turbulence, the eddy lifetime was specified by randomizing the integral scale from an exponential probability density function. Following the work of Wang and Stock (1992), Graham and James (1996) pointed out that in the case when the eddy lifetime, τ_e, is specified to be constant, choice of $\tau_e = 2\tau_L$ ensures dispersion consistency. The latter also concluded that the constant eddy lifetime is to be preferred to the exponential lifetime for CPU time-saving reasons. In the present analysis, the constant eddy lifetime is modeled as follows:

$$\tau_e = 2\tau_L = C_1\frac{(v'_{rms})^2}{\varepsilon}, \tag{11}$$

where C_1 is optimized to be 1.0 in order to give the best fit to the experimental deposition data of Liu and Agarwal (1974). For the sake of simplicity a constant C_1 is adopted here, even though a proper function of the turbulent Reynolds number ($Re_\lambda = u'\lambda/v$) will be better. Note that only relatively small particles ($\tau_p^+ < 1,000$) are considered so that the crossing effect is neglected and consequently the length scale is not directly involved in the simulation. The values of v'_{rms} and ε are evaluated from the equations in Table 1. Note that the lifetime given above is a deterministic quantity as a function of y^+ of the center of eddy at the start of interaction.

The local fluctuating velocities of the eddy are given as follows:

$$(u_e, v_e, w_e) = (N_u u'_{rms}, N_v v'_{rms}, N_w w'_{rms}), \tag{12}$$

where N_u, N_v and N_w are the random numbers generated from a Gaussian probability density function of zero mean and unity standard deviation. These velocity scales of the eddy are generated at the start of each interaction. The random numbers are maintained constant during one interaction, while the respective RMS values are varied according to y^+ of the particle. As shown later, the use of local RMS values, particularly for the wall-normal component, is crucial for adequate prediction of deposition velocities of small particles. In the calculation of particle movement, instantaneous fluid velocities in Eq. (2) are substituted for the sum of mean fluid velocities and the velocities scales of the fluid eddy as, e.g., $u_f = \bar{u}_f + u_e$.

Figs. 5(a) and (b) show the velocity scales and the lifetime, respectively, used in the present study in comparison with the scales used by Schuen et al. (1983) and Kallio and Reeks (1989). The velocity scale of Schuen et al. is close to the present w'_{rms} but substantially larger than the present v'_{rms}. The present (and DNS) v'_{rms} is very close to the velocity scale of Kallio and Reeks, who considered only the wall-normal velocity scale in their simulation. As seen in Fig. 5(b), the present lifetime differs significantly from the lifetimes of Schuen et al. (Eq. (7) with $C_\mu = 0.09$) and Kallio and Reeks both in profile and in magnitude. The present lifetime diminishes rapidly toward the wall. However, it should be mentioned that the present simulations employ a constant lifetime in the region very near the wall as indicated by horizontal lines in Fig. 5(b). This is to avoid 'the stiffness problem', and two different values are finally chosen: $\Delta t = 10^{-7}$ s for $\tau_p^+ < 3$ and $\Delta t = 10^{-6}$ s for $\tau_p^+ \geqslant 3$. The choice of these values are based on the careful examination of the influence of the lifetime on the prediction of

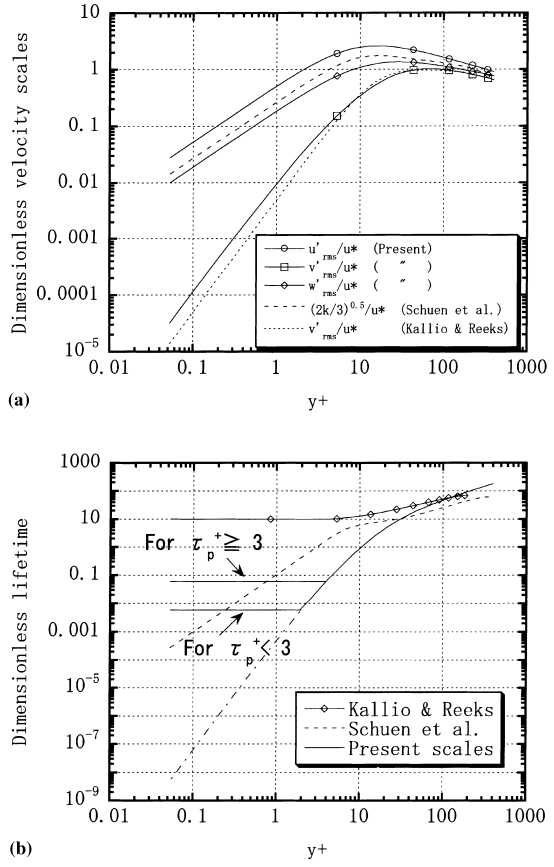

Fig. 5. Characteristic scales of fluid eddies: (a) velocity scales, (b) lifetime.

deposition velocities as described in more detail later. The use of constant lifetime near the wall was already tested by Kallio and Reeks, who chose $\tau_e^+ = 10$ as a typical lifetime of the organized structures in turbulent pipe flows.

2.4. Calculation conditions

The primary flow considered is a fully developed turbulent flow in a vertical pipe having an internal diameter of 12.7 mm, the same as the experiment of Liu and Agarwal (1974). They measured the rate of deposition of monodispersed droplets (uranine-tagged olive oil ranging from 1.4 to 21.0 μm in diameter with 920 kg/m^3 of density) in a vertical, downward air flow (glass pipe with 1.016 m length) at Reynolds numbers of 10,000 and 50,000. Their results of deposition velocities are based on the average over 0.508 m long test section, neglecting the entrance (0–0.254 m) and the exit (0.762–1.016 m) regions.

In the present calculations, thousands (~10,000) of particles (920 kg/m^3) of various diameters (2.0–68.5 μm) are released individually at the entrance of the pipe. Their initial velocities are imposed as follows:

$$u_{p0} = u_f \quad \text{and} \quad v_{p0} = w_{p0} = 0. \tag{13}$$

Subsequent velocities and trajectories of particles are calculated according to the particle equation of motion, until particles impinge on the pipe wall or exceed an axial length (1 m). Particles are assumed to stick on the wall after impingement, which is regarded to happen when the center of a particle reaches a wall-normal distance equal to the radius of the particle.

In order to examine the effect of initial mass concentration distribution of particles, $\bar{C}_0$, on the deposition velocities, two sets of calculations having different release conditions, Runs A and B, are carried out. In Run A, all particles are released from the centerline of the pipe. In Run B, particles are released in such a way that $\bar{C}_0$ becomes uniform over the pipe cross-section. This uniform release is achieved by dividing the pipe cross-section into 10 concentric layers having equal area and by setting the number of particles to be released from each layer according to Eq. (26) with $A/A_i = 10$ and $\bar{C}_i/\bar{C} = 1$. Note that the number of particles to be released from the ith layer, N_{pi}, is proportional to the mean fluid velocity at this layer, $\bar{u}_{fi}$. The number of particles thus determined is given in Table 2. The representative radius of each layer is defined by the radial position of the middle of the layer.

The calculation in the cylindrical coordinate system has a singular point on the centerline of the pipe, where the centrifugal force and the conservation of angular momentum in Eq. (2) will take infinitely large values. In fact, some of the present simulations are found to generate unrealistic particle trajectories when particles approach very close to the centerline of the pipe. To avoid this problem, the calculation in the centerline region ($<0.1d_t$) is done in the Cartesian coordinate system instead of the cylindrical coordinate system. Furthermore, the lift force is neglected and $u'_{x,\mathrm{rms}} = u'_{y,\mathrm{rms}} = v'_{\mathrm{rms}}$ are assumed, where $u'_{x,\mathrm{rms}}$ and $u'_{y,\mathrm{rms}}$ are the RMS values of velocity fluctuations in the cross-sectional directions in the Cartesian coordinate system. These simplifications are based on the consideration that the streamwise mean velocity gradient is low and the RMS values of velocity fluctuations are approximately homogeneous in the centerline region. All calculations were performed on workstations (Alpha chip 21164A, 533 MHz). Each calculation of 10,000 particles released needed 1–65 CPU hours, depending on the diameter of particles.

2.5. Eddy lifetime and calculation time step

The eddy lifetime, τ_e, as given by $(v'_{\mathrm{rms}})^2/\varepsilon$ from Eq. (11) diminishes to infinitesimal values toward the wall in a turbulent pipe flow. This impedes Lagrangian simulation of particle deposition to be done within allowable computation time. To circumvent this stiffness problem, the lowest limit of eddy lifetime is assigned in the present calculation. This is done by introducing a constant time step, Δt, for the integration of Eq. (2) and by setting $\tau_e = \max(\Delta t, (v'_{\mathrm{rms}})^2/\varepsilon)$. This is equivalent to defining a profile of eddy lifetime that becomes constant near the wall as shown in Fig. 5(b). In consequence, the present profile of eddy lifetime becomes similar to that used by Kallio and Reeks (1989), except for that their lifetime near the wall is

Table 2
Number of particles released at different concentric layers in Run B

Layer	Representative radius (m)	Number of particles
1	0.0010	1191
2	0.0024	1145
3	0.0032	1114
4	0.0037	1084
5	0.0043	1052
6	0.0047	1015
7	0.0051	973
8	0.0055	918
9	0.0059	838
10	0.0062	672
Total		10002

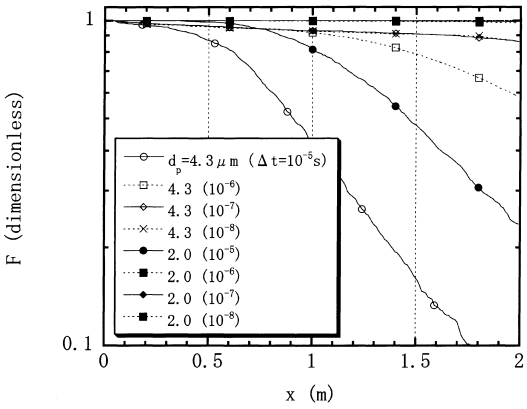

Fig. 6. Influence of time steps, Δt, on the fraction of particles remaining in the flow.

more than two orders of magnitude larger than the present values.

To check the influence of the time step on the prediction of particle depositions, the value of Δt was decreased from 1×10^{-5} to 1×10^{-8} s. Fig. 6 gives the result of the fraction of particles remaining in the flow, F, simulated with various time steps. F is evaluated by counting the number of particles that reach the sampling cross-section as follows:

$$F = \frac{\text{the number of crossing particles}}{\text{the total number of released particles}}.$$

It is seen that the axial variations of F for $d_p = 2.0$ and 4.3 μm ($\tau_p^+ = 0.7$ and 3.0, respectively) change substantially with reduction of Δt from 10^{-5} to 10^{-7} s but become almost invariable for further reduction from 10^{-7} to 10^{-8} s. However, the axial variations within 1 m long upstream test section (i.e, $x = 0$–1.0 m) become already invariable for $\Delta t \leqslant 10^{-6}$ s. Not shown here, the effect of Δt is less significant for larger particles than those examined in Fig. 6. For these reasons, $\Delta t = 10^{-7}$ s ($\Delta t^+ = 5.9 \times 10^{-3}$) and 10^{-6} s ($\Delta t^+ = 5.9 \times 10^{-2}$) are chosen, respectively for $d_p < 4.3$ and $d_p \geqslant 4.3$ μm so that the present results become independent of the time step chosen.

2.6. Particle concentration and deposition velocity

Ueda (1981) has shown that the rate of deposition of particles is given by

$$m_p = k_p(\bar{C} - C_0), \tag{14}$$

where k_p is the deposition mass transfer coefficient, generally referred to as the particle deposition velocity, $\bar{C}$ is the bulk mean particle concentration and C_0 is the particle concentration at the wall. Assuming that C_0 is zero and there is no reemission of particles, we have

$$m_p = k_p\bar{C}. \tag{15}$$

Considering the flow model shown in Fig. 7, the mass flow rates of fluid and particles passing through the cross-sectional area, A, are, respectively

$$M_f = \rho_f(1 - \chi_p)A\bar{u}_f \quad \text{and} \quad M_p = \rho_p\chi_pA\bar{u}_p, \tag{16}$$

where $\bar{u}_f$ and $\bar{u}_p$ are the average velocities and χ_p is the volume fraction of particles, which is the same as the fraction of cross-sectional area occupied by the particles as depicted in the figure.

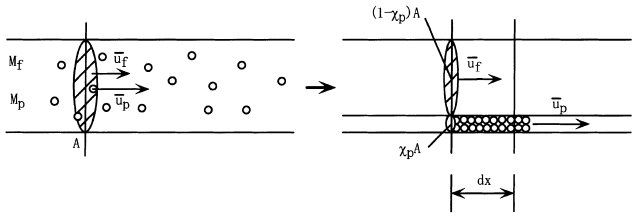

Fig. 7. Flow model of fluid and particles.

The volumetric capacity of the flow over a small increment of the tube length, dx, is related to the mass flow rates as follows:

$$A\,\mathrm{d}x = (1 - \chi_p + \chi_p)A\,\mathrm{d}x = \left(\frac{M_f}{\rho_f\bar{u}_f} + \frac{M_p}{\rho_p\bar{u}_p}\right)\mathrm{d}x. \tag{17}$$

Then, we have the particle average concentration from Eqs. (16) and (17) as follows:

$$\bar{C} \equiv \frac{\rho_p\chi_pA\,\mathrm{d}x}{A\,\mathrm{d}x} = \frac{M_p}{\frac{M_f}{\rho_f}\frac{\bar{u}_p}{\bar{u}_f} + \frac{M_p}{\rho_p}}. \tag{18}$$

If $\rho_p \gg \rho_f$, then

$$\bar{C} = \rho_f\frac{M_p}{M_f}\frac{\bar{u}_f}{\bar{u}_p}. \tag{19}$$

A mass balance over dx where deposition is occurring leads to

$$\frac{\mathrm{d}M_p}{\mathrm{d}x} = -\pi\,d_tm_p = -\pi\,\mathrm{d}_tk_p\rho_f\frac{M_p}{M_f}\frac{\bar{u}_f}{\bar{u}_p}. \tag{20}$$

If $\bar{u}_f/\bar{u}_p$ is considered to be unity, the particle deposition velocity can be obtained by:

$$k_p = \frac{M_f}{\pi\,d_t(x_2 - x_1)\rho_f}\ln\left[\frac{M_{p1}}{M_{p2}}\right], \tag{21}$$

where subscripts 1 and 2 denote the values at x_1 and x_2, respectively. The particle deposition velocity is evaluated by rewriting the above equation as follows:

$$k_p = \frac{M_f}{\pi\,d_t(x_2 - x_1)\rho_f}\ln\left[\frac{M_{p1}}{M_{p2}}\right] = \frac{\bar{u}_fd_t}{4(x_2 - x_1)}\ln\left[\frac{F_1}{F_2}\right]. \tag{22}$$

The above replacement of M_{p1}/M_{p2} by F_1/F_2 is due to the fact that the mass flow rate of particles at a cross-section is proportional to the number of particles passing through that cross-section.

3. Results and discussion

3.1. Particle deposition velocity

The fraction of particles remaining in the flow, F, calculated for various diameters (2.0–68.5 μm) in Run A is shown in Fig. 8(a), and the values of F are summarized in Table 3 along with the values of τ_p^+ and Δt^+. For 68.5 μm diameter particles, approximately 20% of the released particles still remain in the flow at $x = 1$ m, meaning therefore that about 80% of the particles have deposited on the wall. The particle deposition velocities determined using Eq. (22) are presented in dimensionless form, k_p/u^*, in Fig. 8(b), where $x_2 - x_1$ in Eq. (22) is taken to be 0.5 m to evaluate locally averaged k_p/u^*. It is seen that k_p/u^* first increases and gradually approaches to a developed value. The entrance length varies from one particle diameter to another, and some particles (e.g., $d_p = 5.8$ μm and

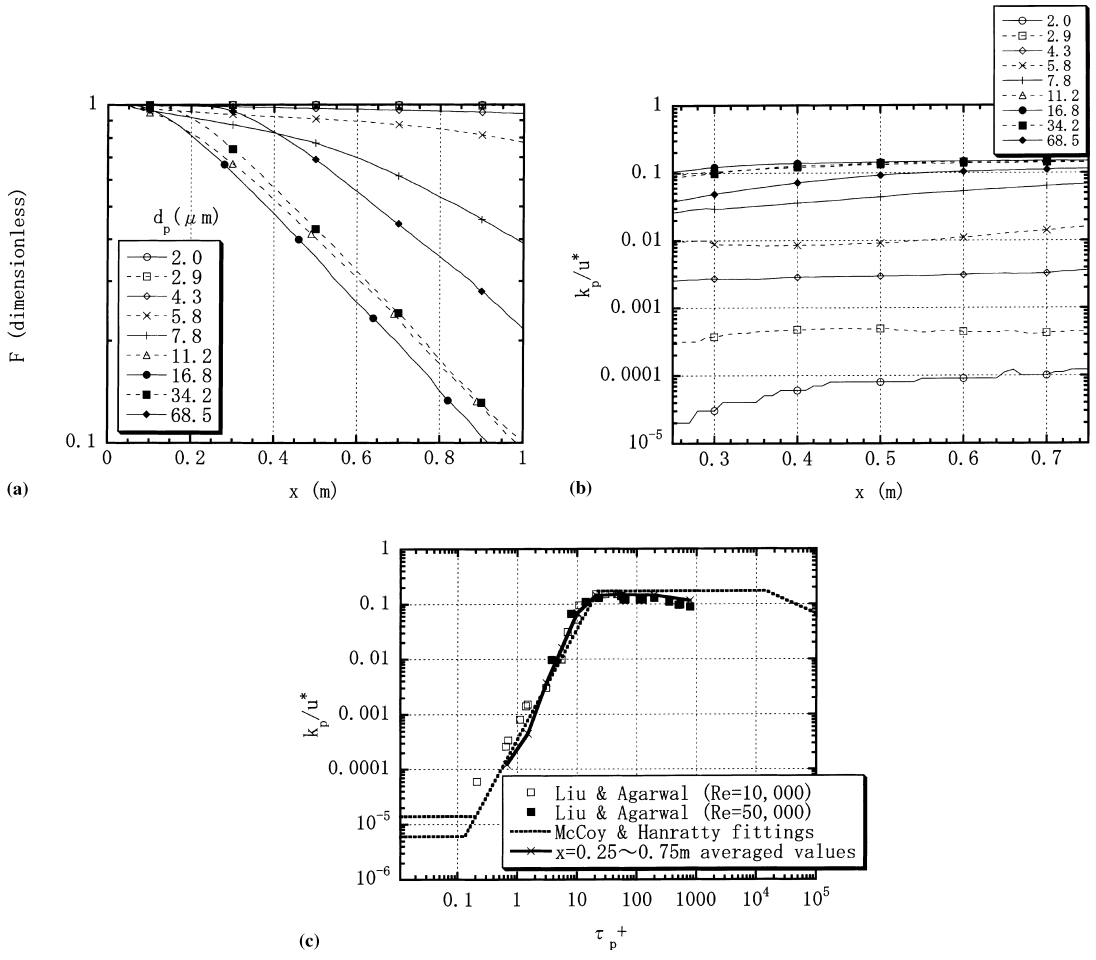

Fig. 8. Run A (centerline release): (a) fraction of particles remaining in the flow versus the pipe length, (b) dimensionless particle deposition velocity k_p/u^* locally averaged over 0.5 m of pipe length, (c) k_p/u^* versus the dimensionless particle relaxation time τ_p^+.

7.8 μm) seem to be still developing at the exit of the test section while smaller particles ($d_p \leqslant 4.3$ μm) seem to have reached an equilibrium state of deposition.

In Fig. 8(c), the present result of the particle deposition velocities evaluated for $x = 0.25 \sim 0.75$ m are shown in solid line and compared with experimental data reported by Liu and Agarwal (1974) as well as with the fittings reported by McCoy and Hanratty (1977). Very good agreement is obtained between the present calculation and the measurement of Liu and Agarwal for the entire range of τ_p^+. Interestingly, both the present calculation and the measurement of Liu and Agarwal start to deviate from a horizontal line (i.e., $k_p/u^* = 0.17$) of the McCoy and Hanratty fittings at around $\tau_p^+ = 100$. A similar deviation is also reported by Uijttewaal and Oliemans (1996)

Table 3
Fraction of particles remaining in the flow as function of the axial location for various diameters ($d_p = 2.0$–68.5 μm) or relaxation times ($\tau_p^+ = 0.7$–773.3) in Run A (centerline release)

	d_p (μm)	2.0	2.9	4.3	5.8	7.8	11.2	16.8	34.2	68.5
	τ_p^+	0.7	1.4	3.0	5.5	10.0	20.7	46.5	192.8	773.3
	Δt^+	5.9×10^{-3}	5.9×10^{-3}	5.9×10^{-3}	5.9×10^{-2}	5.9×10^{-2}	5.9×10^{-2}	5.9×10^{-2}	5.9×10^{-2}	5.9×10^{-2}
x (m)	0.0	1	1	1	1	1	1	1	1	1
	0.1	1	0.9999	0.9966	0.9751	0.9633	0.9496	0.9705	0.9997	1
	0.2	1	0.9997	0.9926	0.9545	0.9175	0.824	0.8119	0.915	0.9994
	0.3	1	0.9988	0.9867	0.9377	0.8742	0.6693	0.6307	0.7409	0.9557
	0.4	1	0.9977	0.9819	0.9224	0.826	0.524	0.4766	0.569	0.8312
	0.5	0.9998	0.9969	0.9751	0.909	0.7718	0.4035	0.3552	0.4289	0.6888
	0.6	0.9996	0.9954	0.9697	0.8939	0.6962	0.3062	0.2593	0.3206	0.5531
	0.7	0.9992	0.9948	0.9632	0.873	0.6159	0.2317	0.1967	0.2413	0.4442
	0.8	0.9991	0.9943	0.957	0.8474	0.5326	0.1706	0.1423	0.1766	0.3547
	0.9	0.9989	0.9932	0.9497	0.8129	0.4576	0.1297	0.1048	0.1315	0.2797
	1.0	0.9986	0.9925	0.9397	0.774	0.3881	0.0948	0.0793	0.1003	0.2164

in their DNS and LES results. It is worth pointing out that the decreasing behavior of k_p/u^* with increasing τ_p^+ for $\tau_p^+ > 100$ is discernible in the data compiled by McCoy and Hanratty (Fig. 1 in their paper), although they proposed a constant deposition velocity as the best fit to all data taken from different experiments.

Fig. 9 shows the particle deposition velocities for Run B, in which particles are released uniformly over the pipe cross-section. It is recognized from comparison between Figs. 8(c) and 9(b) that the particle release conditions can affect the deposition velocity of small particles ($\tau_p^+ < 10$) but have negligible influence on the deposition velocity of large particles ($\tau_p^+ > 20$). In fact, the deposition velocities for $\tau_p^+ = 0.7$ and 1.4 predicted in Run B (uniform release) are lower than those predicted in Run A (centerline release), while the deposition velocities for $\tau_p^+ = 3$ and 5.5 predicted in Run B are higher than those predicted in Run A. Examination of Figs. 8(b) and 9(a) reveals that the deposition velocities of small particles (particularly, $d_p = 5.8$–7.8 μm) are not yet at their fully developed state at the exit of the 1 m long test section and that the developing rate is dependent on τ_p^+. These complicated behaviors are found to be related to the 'near-wall build-up' of small particles as discussed in more detail later. The present results may lead to the conclusion that the length of the test section can be a factor that affects the deposition velocities of small particles. This implies that the total computation time in DNS and LES in the prediction of particle deposition can also be a factor affecting the deposition velocities of small particles.

The influence of velocity scales and lifetime of fluid eddies on the prediction of particle deposition velocities is shown in Fig. 10. The dashed line in the figure is the prediction by Schuen's k–ε turbulence model. The use of their characteristic scales (Eq. (7)) leads to a considerable overestimate of particle deposition velocities for $\tau_p^+ < 10$ and leads to an appreciable underestimate for $\tau_p^+ > 10$. To see the importance of the velocity scales, the Schuen's velocity scales are replaced by the present velocity scales determined by DNS fitting. The prediction for $\tau_p^+ < 10$ is remarkably improved by this replacement, but the prediction for $\tau_p^+ > 10$ is still unsatisfactory. In consequence, the replacement of the eddy lifetime is also needed to have a good prediction for entire range of τ_p^+. The above examination has demonstrated that the Lagrangian eddy–particle interaction model itself is capable of predicting particle deposition velocities if adequate velocity scales and lifetime of fluid eddies are used in the simulation.

The effect of various other factors on the prediction of deposition velocities is examined and presented in Fig. 11. In Case 1 denoted by 'no local vel. scales' in the figure, the velocity scales are not locally varied but fixed throughout one interaction, and all other conditions are set identical to those of Run A. In this calculation, small particles are found to impinge on the wall more frequently when a large radial velocity fluctuation is generated at the start of new interaction, resulting in an erroneous increase of deposition velocity for $\tau_p^+ < 3$. In Case 2 denoted by 'no centrifugal forces' in the figure, it is recognized that excluding the centrifugal force and the conservation of angular momentum from the particle equation of motion leads to an appreciable underestimate of the deposition velocity for large particles ($\tau_p^+ > 20$). This is because any spanwise displacement of particles should result in their approaching toward the wall in the pipe geometry but the negligence of the centrifugal force and the conservation of angular momentum can no longer represent such effect. In Case 3 denoted by 'no lift' in the figure, it is found that excluding the corrected Saffman lift force from the particle equation of motion considerably reduces the deposition velocities for $5 \leqslant \tau_p^+ < 200$. The deposition velocities for smaller

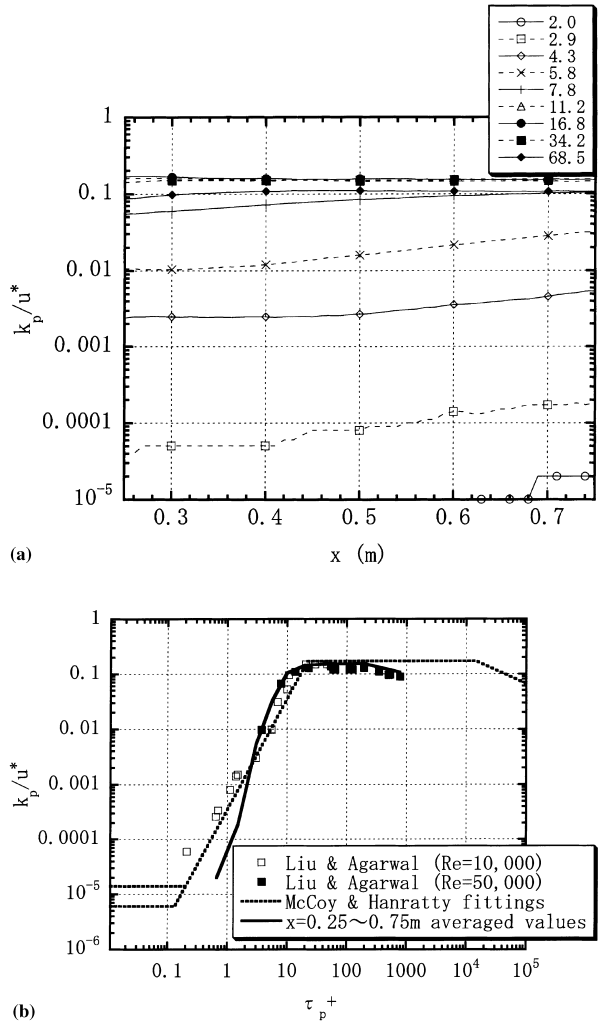

Fig. 9. Run B (uniform release): (a) dimensionless particle deposition velocity k_p/u^* locally averaged over 0.5 m of pipe length, (b) k_p/u^* versus the dimensionless particle relaxation time τ_p^+.

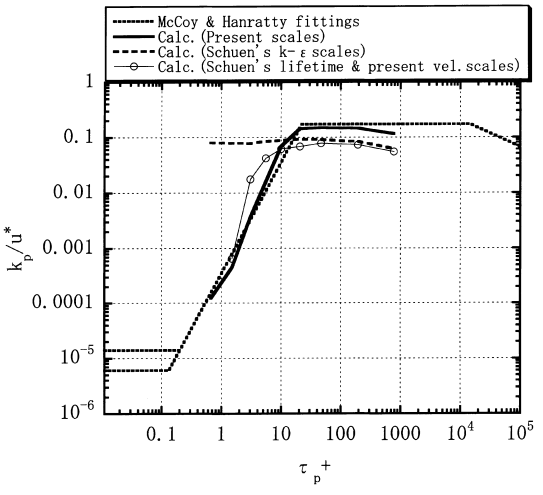

Fig. 10. Influence of velocity scales and lifetime of fluid eddies on the prediction of particle deposition velocities.

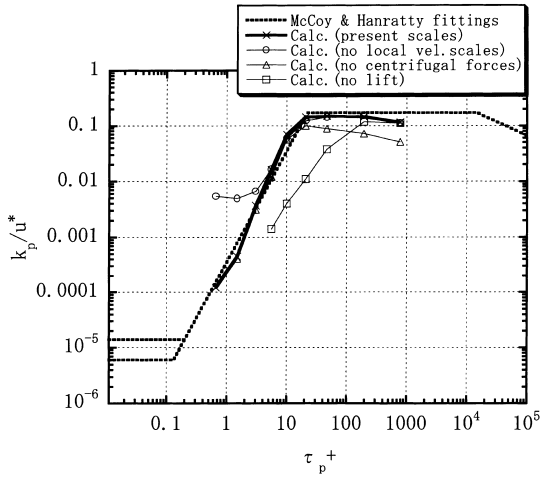

Fig. 11. Effect of exclusion of variable local velocity, Saffman lift force or centrifugal force and conservation of angular momentum.

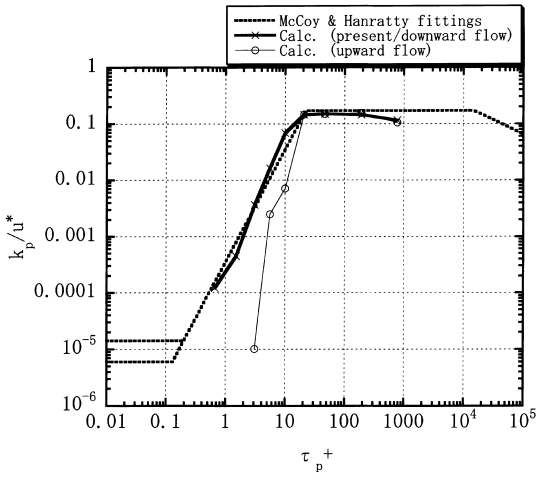

Fig. 12. Effect of flow direction on particle deposition velocities.

particles ($\tau_p^+ \leqslant 3.0$) are not included in the figure because the number of particles deposited on the wall during the simulation is too small to be taken as statistically valid. This, however, implies that the deposition velocities for those smaller particles also decrease in the absence of the lift force in the present simulation. These results of reduced deposition are consistent with the existence of wall-ward lift force acting on heavy particles in vertically downward flows. Uijttewaal and Oliemans (1996) reported a considerable decrease, approximately by a factor of three, in the deposition velocities for $5 \leqslant \tau_p^+ \leqslant 40$ when the lift force given by McLaughlin (1991) is omitted from the particle equation of motion, and the present results are in qualitative agreement with their results.

Wang et al. (1997) have reported that the modified expressions for lift force incorporated into their LES of particle deposition in a turbulent channel flow lead to negligible influence of lift force on the rate of deposition of very small particles ($\tau_p^+ < 2$) but result in considerable reduction, approximately by a factor of five, of the rate of deposition of larger particles ($6 < \tau_p^+ < 300$). The present result is in agreement with that of Wang et al. as for the reduction of deposition velocity for larger particles even though the present approach, which is based on McLaughlin (1991), is simpler for implementation into simulations based on RANS equations. On the other hand, the decrease of deposition velocities implied for $\tau_p^+ \leqslant 3.0$ in the present simulation is not consistent with the result of Wang et al. At present, the clarification of this discrepancy encounters difficulties because (1) the deposition velocities for those small particles show considerable scatters (Fig. 1) and (2) the approach used by Wang et al. seems to be sensitive to small changes in the expressions or simulation conditions as recognized from that Chen and McLaughlin (1995) predicted using DNS $k_p/u^* = 0.5 \times 10^{-5}$ for $\tau_p^+ = 1$ while Wang et al. (1997) predicted using LES $k_p/u^* = 10 \times 10^{-5}$ for the same τ_p^+. It should be noted that the present negligence of Brownian motions can lead to unrealistically small deposition velocities for very small particles. In addition, the present simulation is not free of 'spurious build-up' of fluid particles, which is inherent in random-walk approach as described in detail later, making the interpretation of the effect of the lift force on the rate of deposition of very small particles further difficult.

Fig. 12 shows the effect of flow direction on the deposition velocities. The present main calculation is made for downward flow, the same as in the experiment of Liu and Agarwal (1974). In upward flows, gravity causes heavy particles ($\rho_p \gg \rho_f$) to have lower axial velocities than the surrounding fluid. This will result in the corrected Saffman lift force pushing particles, particularly small particles, away from the wall. This is the reason for the reduced deposition velocities for small particles ($\tau_p^+ < 20$) as seen in the figure. Note that the present data point for $\tau_p^+ = 3.0$ showing very small deposition velocity should be taken with reservation for the same reasons mentioned above.

The effect of particle density on the deposition velocity is presented in Fig. 13. The simulation conditions are identical to those of Run A except for the change of particle density. It is seen that there is little influence of particle density on the deposition velocities for large particles ($\tau_p^+ > 20$) but a notable influence for smaller particles in the case of $\rho_p/\rho_f = 5,000$. However, the deposition velocities for $\rho_p/\rho_f = 770$ and 500 are almost the same for the entire range of τ_p^+. The deposition is regarded to occur when the distance between the center of a particle and the pipe wall becomes equal to the radius of the particle. For the same τ_p^+ and under the same flow conditions, the radius of a particle is inversely proportional to the square root of the density of the particle (i.e., $d_p \propto \sqrt{\tau_p^+/\rho_p}$), meaning that high-density particles need to be drifted closer to the wall than low-density particles until they are deposited on the wall. This is the reason for the reduced deposition velocities for

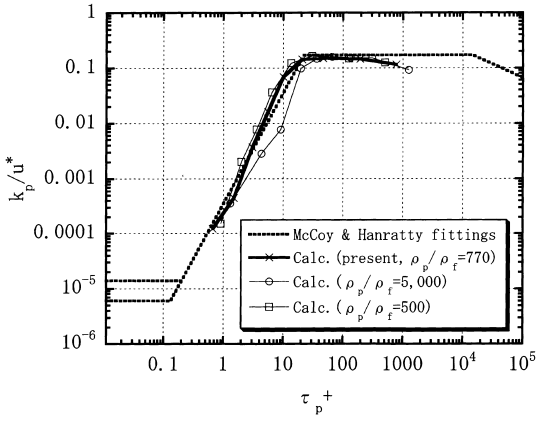

Fig. 13. Effect of particle density on particle deposition velocity.

$\rho_p/\rho_f = 5000$. In downward flows, however, this effect of particle density is somewhat canceled by the effect of lift force because the wall-ward lift force acts on high-density particles near the wall.

3.2. Concentration of particles

The profile of mass concentration of particles is obtained in the present simulation by dividing the pipe cross-section into 40 concentric sampling layers, each having equal cross-sectional area. Combining Eqs. (16) and (19), the mass concentration of the ith layer is evaluated as follows:

$$\bar{C}_i = \frac{\rho_p \chi_{pi}}{1-\chi_{pi}} = \frac{\rho_p N_{pi} \pi d_p^3/6}{(\Delta t_s)\bar{u}_{pi}A_i - N_{pi}\pi d_p^3/6}, \tag{23}$$

where N_{pi} is the number of particles sampled during Δt_s, A_i the cross-sectional area and Δt_s the sampling period, which is set to be long enough for the slowest particle released to reach the sampling cross-section. Note that the relation $\chi_{pi} = N_{pi}(\pi d_p^3/6)/(\Delta t_s \bar{u}_{pi} A_i)$ is used in the above derivation. In dilute suspensions, Eq. (23) can be simplified as follows:

$$\bar{C}_i = \frac{\rho_p N_{pi} \pi d_p^3/6}{(\Delta t_s)\bar{u}_{pi}A_i}. \tag{24}$$

Similarly, the average mass concentration is given by

$$\bar{C} = \sum_i \bar{C}_i \frac{A_i}{A} = \frac{\rho_p \pi d_p^3/6}{(\Delta t_s)A} \sum_i \frac{N_{pi}}{\bar{u}_{pi}}, \tag{25}$$

where A is the entire pipe cross-section. It can be shown that the above equation is reduced to Eq.(19) if $\bar{u}_{pi}$ is represented by $\bar{u}_p$. The dimensionless mass concentration is then obtained as follows:

$$\frac{\bar{C}_i}{\bar{C}} = \frac{N_{pi}/\bar{u}_{pi}}{\sum_i (N_{pi}/\bar{u}_{pi})} \frac{A}{A_i}. \tag{26}$$

In inhomogeneous turbulent flows, particles tend to move from high turbulence regions to low turbulence regions by the driving force named 'turbophoresis' by Reeks (1983). The driving force in fully developed turbulent pipe flows is the radial gradient of turbulence intensity of radial velocity fluctuations, resulting in the near-wall build-up of particles for $1 \leqslant \tau_p^+ \leqslant 100$ as shown by Young and Leeming (1997) in their theoretical considerations and Eulerian-based simulations. The magnitude of the near-wall build-up is determined by the balance between the supply of particles due to turbophoresis and their consumption due to deposition, therefore providing the most severe test for simulations of particle depositions. MacInnes and Bracco (1992) pointed out that the random-walk approach would generate 'spurious build-up' of fluid particles, which should not be accumulated into any regions because of the continuity conditions. As the continuity conditions are the consequence of mutual interaction (or two-way coupling) among fluid particles themselves, the random-walk approach based on one-way coupling needs to introduce a sort of artificial counter-turbophoresis into the particle equation of motion to keep fluid particles dispersed uniformly in the turbulent flows. However no treatment has been incorporated into the present simulation because currently proposed approaches such as those of Wilson et al. (1981) and MacInnes and Bracco (1992) are found not to result in satisfactory improvement. Underwood (1993) also proposed a method to avoid the spurious build-up of particles, but the counter-turbophoresis introduced by the method seemed to be too excessive to reproduce true build-up that occurs near the wall for particles in the range of $1 \leqslant \tau_p^+ \leqslant 100$. In consequence, the present simulation is not free of the spurious build-up of fluid particles near the wall, leading to the statement that the present deposition velocities predicted for very small particles (say, $d_p \leqslant 4.3$ μm or $\tau_p^+ \leqslant 3$), which behave like fluid particles to some extent, should be accepted with reservation. Nevertheless, it is believed that the deposition velocities for those particles are not strong functions of the magnitude of near-wall build-up as judged from their equilibrium state of deposition velocities for $d_p \leqslant 4.3$ μm as shown in Fig. 8(b).

The dimensionless mass concentration profiles predicted in Run A are plotted in Fig. 14. These profiles for $\tau_p^+ = 1000$, 100 and 10 are obtained at the sampling cross-section located at $x = 0.5$ m. For comparison, the results obtained by Young and Leeming (1997) are also shown in the figure. They have proposed an Eulerian approach using turbulent diffusion and turbophoresis correlations. Present calculations show that relatively large particles ($\tau_p^+ = 1000$, 100) have a flat profile in the core of the pipe, indicating that the transport of particles in this region is due to turbulent diffusion. The deposition of large particles is rather insensitive to the near-wall turbulence because their large inertia allows them to penetrate the viscous sublayer and impinge on the wall by a free flight mechanism. In contrast, small particles seem to have different behavior, showing 'near-wall build-up' as seen in the profile for $\tau_p^+ = 10$. Small particles also move toward the wall via turbulent diffusion, but their movement is dumped near the wall due to their small inertia. In consequence, they stay near the wall longer than large particles before impinging onto the wall. Agreement between Young and Leeming and the present is very good for $\tau_p^+ = 100$ and acceptable for $\tau_p^+ = 10$ and 1000. The near-wall build-up of small particles is also reported by Kallio and Reeks (1989), Chen and McLaughlin (1995) and Uijttewaal and Oliemans (1996) in their numerical simulations of particle deposition, although the magnitude of build-up differs considerably from one another.

The positions of particles that have reached the sampling cross-section at $x = 0.5$ m are displayed in Fig. 15, in which the near-wall build-up for $\tau_p^+ = 10$ is clearly observed along with the relative accumulation in the core of the pipe.

Fig. 16 shows the dispersion of particles in the radial direction (i.e., variance of radial displacement of particles) predicted in Run A (centerline release). Large particles ($\tau_p^+ = 1000$ and 100) have a relatively short developing length before reaching a nearly constant dispersion. This is consistent with the dimensionless mass concentration profile, $\bar{C}_i/\bar{C}$, being near unity over the pipe cross-section at $x = 0.5$ m. On the other

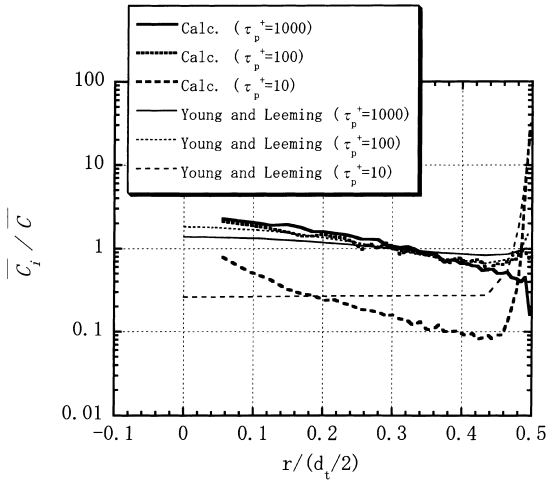

Fig. 14. Profiles of dimensionless mass concentration of particles.

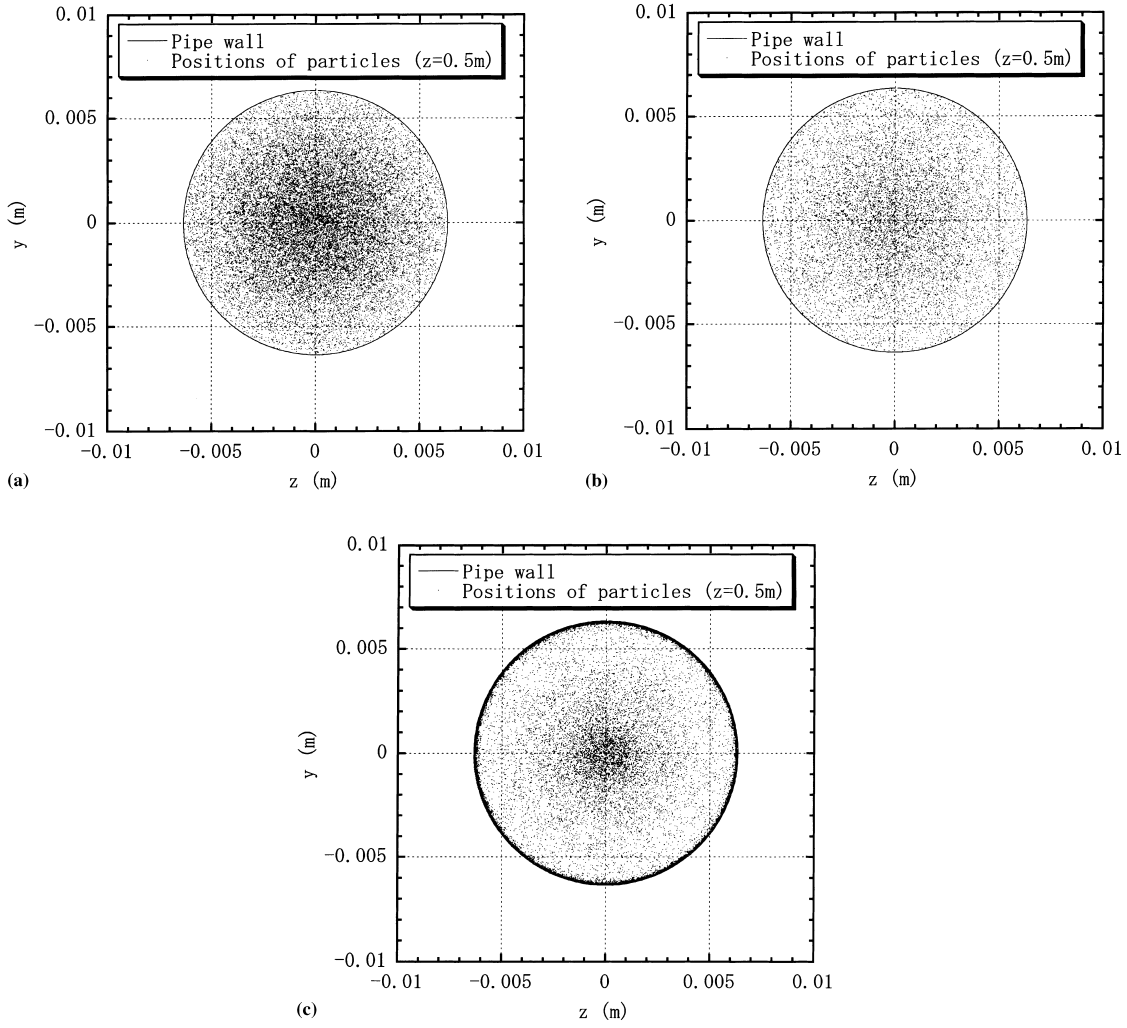

Fig. 15. Position of particles at 0.5 m section from releasing point. $\tau_p^+ = 1000$ (a), 100 (b), 10 (c).

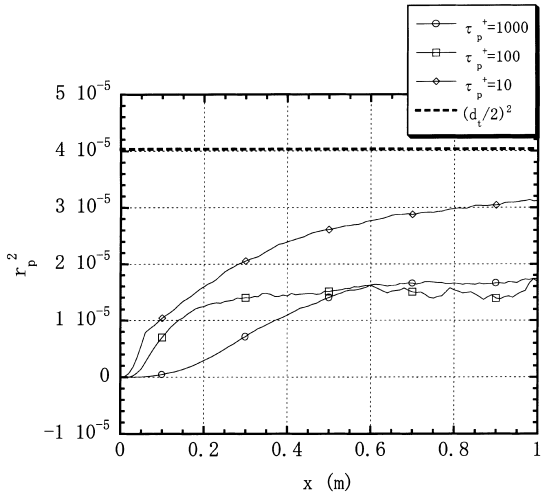

Fig. 16. Dispersion of particles in the radial direction.

hand, the dispersion of small particles ($\tau_p^+ = 10$) is still in development at the exit of the pipe test section and is showing to asymptote to $(d_t/2)^2$. This may suggest that small particles continue to accumulate near the wall until most of them are trapped there. Experimental confirmation of this interesting phenomenon seems to be insufficient, but it is worth pointing out that Sun and Lin (1986) experimentally observed the near-wall build-up of very small particles ($\tau_p^+ = 0.020$–0.3) in a horizontal turbulent duct flow.

4. Conclusions

The present study has demonstrated that the one-way coupling Lagrangian eddy–particle interaction model is able to predict adequately the rate of deposition of particles onto the wall in a turbulent pipe flow for a wide range of particle relaxation time ($3 < \tau_p^+ < 770$). To achieve adequate predictions, however, the proper representation of the velocity and the timescales of the primary flow is crucial. In fact, the use of a conventional k–ε turbulence model associated with the isotropic decomposition of turbulence kinetic energy is shown to lead to an unsatisfactory prediction. In the present simulation, the velocity and timescales determined from curve fitting to the DNS data of turbulent channel flow are used to predict the rate of deposition successfully. Although the RANS equations at their present stage are not capable of providing accurate turbulence statistics especially for complex turbulent flows, it may be foreseen that the combined use of the RANS equations

with newly emerging experimental techniques such as particle image velocimetry will open up a practical way for predicting reliable turbulence statistics through careful optimization of the parameters in the RANS equations adopted. In this respect, although it is post-predictive currently, the present statistical simulation can be considered as a predictive tool for particle depositions in turbulent flows.

Influence of particle inlet conditions, namely initial particle concentration distributions, is examined for the first time in the present study. Two different conditions, centerline release and uniform release, are considered. It is found that although the inlet condition has no significant influence on the rate of deposition of large particles ($20 < \tau_p^+ < 770$), it has an appreciable influence on smaller particles. This is related to the difference in the rate of dispersion; small particles need long traveling distance until they reach a fully-dispersed state while large particles reach that state quickly. This suggests that the rate of deposition is dependent on the length of the pipe test section used in the experiment. Special care must, therefore, be paid to the inlet conditions if one is measuring the deposition rate of small particles.

The effect of various terms in the particle equation of motion on the rate of deposition is examined. It is shown that the effect of the Saffman lift force is considerable, and that the present treatment using McLaughlin's model (1991) and average velocity gradients of the fluid flow is adequate for the flow conditions examined, although further analysis is necessary, particularly the inclusion of the wall-induced effect on the lift force as proposed by Chen and McLaughlin (1995) must be considered. The exclusion of the centrifugal force and the conservation of angular momentum deteriorates the prediction for $\tau_p^+ > 20$. The flow direction, upward or downward, also has a notable influence on relatively small particles ($\tau_p^+ < 20$), showing that the rate of deposition is reduced appreciably in upward flows.

The present calculation reproduces the 'near-wall build-up' of small particles as found in some previous simulations. Since few experimental verifications of this unique phenomenon have yet been made, future experimental efforts are desirable. It should be stated that the present simulation is not free of 'spurious build-up' of fluid particles, which is known to be inherent in the random-walk approach, and therefore that the present results for very small particles (say, $\tau_p^+ \leqslant 3$) should be accepted with reservation. As noted by one of the reviewers, the elimination of the spurious drift is a difficult issue and further rigorous study is required to confront this problem.

Acknowledgements

This work was supported by Grant-in-Aid for Scientific Research (C) (No. 09650230) of the Ministry of Education, Science, Sports and Culture of Japan.

References

Antonia, R.A., Teitel, M., Kim, J., Browne, L.W.B., 1992. Low-Reynolds-number effects in a fully developed turbulent channel flow. J. Fluid Mech. 236, 579–605.

Beal, K.S., 1970. Deposition of particles in turbulent flow on channel or pipe walls. Nucl. Sci. Engrg. 40, 1–11.

Berlemont, A., Desjonqueres, P., Gousbet, G., 1990. Particle Lagrangian simulation in turbulent flows. Int. J. Multiphase Flow 16 (1), 19–34.

Burry, D., Bergeles, G., 1993. Dispersion of particles in anisotropic turbulent flows. Int. J. Multiphase Flow 19 (4), 651–664.

Chen, M., McLaughlin, J.B., 1995. A new correlation for the aerosol deposition rate in vertical ducts. J. Colloid Interface Sci. 169, 437–455.

Corrsin, S., Lumley, J., 1956. On the equation for a particle in turbulent fluid. Appl. Sci. Res. A, 6, 114–116.

Dreeben, T.D., Pope, S.B., 1997. Probability density function and Reynolds-stress modeling of near-wall turbulent flows. Phys. Fluids 9 (1), 154–163.

Friedlander, S.K., Johnstone, H.F., 1951. Deposition of suspended particles from turbulent gas streams. Ind. Engrg. Chem. 49 (7), 1151–1156.

Ganic, E.N., Mastanaiah, K.M., 1981. Investigation of droplet deposition from a turbulent gas stream. Int. J. Multiphase Flow 7, 401–422.

Gosman, A.D., Ioannides, E., 1981. Aspects of computer simulation of liquid-fueled combustors. Paper AIAA-81-0323, AIAA 19th Aerospace Sci. Meeting, St. Louis, MO.

Govan, A.H., Hewitt, G.F., Ngan, C.F., 1989. Particle motion in a turbulent pipe flow. Int. J. Multiphase Flow 15 (3), 471–481.

Graham, D.I., James, P.W., 1996. Turbulent dispersion of particles using eddy interaction models. Int. J. Multiphase Flow 22 (1), 157–175.

Hinze, J.O. (Ed.), 1975. Turbulence. McGraw-Hill, New York, pp. 460–471.

Hutchinson, P., Hewitt, G.F., Dukler, A.E., 1971. Deposition of liquid or solid dispersions from turbulent gas streams: a stochastic model. Chem. Engrg Sci. 26, 419–439.

Kallio, G.A., Reeks, M.W., 1989. A numerical simulation of particle deposition in turbulent boundary layers. Int. J. Multiphase Flow 15 (3), 433–446.

Lee, S.L., Wiesler, M.A., 1987. Theory on transverse migration of particles in a turbulent two-phase suspension due to turbulent diffusion. Int. J. Multiphase Flow 13 (1), 99–111.

Liu, B.Y.H., Agarwal, J.K., 1974. Experimental observation of aerosol deposition in turbulent flow. Aerosol Sci. 5, 145–155.

Maxey, M.R., Riley, J.J., 1983. Equation of motion for a small rigid sphere in a nonuniform flow. Phys. Fluids 26 (4), 883–889.

McCoy, D.D., Hanratty, T.J., 1977. Rate of deposition of droplets in annular two-phase flow. Int. J. Multiphase Flow 3, 319–331.

MacInnes, J.M., Bracco, F.V., 1992. Stochastic particle dispersion modeling and the tracer-particle limit. Phys. Fluids A 4 (12), 2809–2824.

McLaughlin, J.B., 1991. Inertial migration of a small sphere in linear shear flows. J. Fluid Mech. 224, 261–274.

McLaughlin, J.B., 1993. The lift on a small sphere in wall-bounded linear shear. J. Fluid Mech. 246, 249–265.

Mei, R., 1996. Velocity fidelity of flow tracer particles. Exp. Fluids 22, 1–13.

Mollinger, A.M., Nieuwstadt, F.T.M., 1996. Measurement of the lift force on a particle fixed to the wall in the viscous sublayer of a fully developed turbulent boundary layer. J. Fluid Mech. 316, 285–306.

Reeks, M.W., 1983. The transport of discrete particle in inhomogeneous turbulence. J. Aerosol Sci. 14 (6), 729–739.

Saffman, P.G., 1965. The lift on a small sphere in a slow shear flow. J. Fluid Mech. 22 (2), 385–400.

Sato, Y., Yamamoto, K., 1987. Lagrangian measurement of fluid-particle motion in an isotropic turbulent field. J. Fluid Mech. 175, 183–199.

Schuen, J.S., Chen, L.D., Faeth, G.M., 1983. Evaluation of a stochastic model of particle dispersion in a turbulent round jet. AIChE J. 29 (1), 167–170.

Sun, Y.F., Lin, S.P., 1986. Aerosol concentration in a turbulent flow. J. Colloid Interface Sci. 113 (2), 315–320.

Ueda, T., 1981.Two-phase flow (heat and mass transfer). Yokendo Publication. (in Japanese), pp. 156–174.

Uijttewaal, W.S.J., Oliemans, R.V.A., 1996. Particle dispersion and deposition in direct numerical and large eddy simulations of vertical flows. Phys. Fluids 8 (10), 2590–2604.

Underwood, B.Y., 1993. Random-walk modeling of turbulent impaction to a smooth wall. Int. J. Multiphase Flow 19 (3), 485–500.

Yang, Z.W., Lee, S.L., 1991. On the droplet deposition and mist supercooling in a turbulent channel flow. Part. Part. Syst. Charact. 8, 72–78.

Young, J., Leeming, A., 1997. A theory of particle deposition in turbulent pipe flow. J. Fluid Mech. 340, 129–159.

Wang, Q., Squires, K.D., Chen, M., McLaughlin, J.B., 1997. On the role of the lift force in turbulence simulations of particle deposition. Int. J. Multiphase Flow 23 (4), 749–763.

Wang, L.-P., Stock, D.E., 1992. Stochastic trajectory models for turbulent diffusion: Monte Carlo process versus Markov chains. Atmosphere. Environ. 26A, 1599–1607.

Wilson, J.D., Thurtell, G.W., Kidd, G.E., 1981. Numerical simulation of particle trajectories in inhomogeneous turbulence, II: Systems with variable turbulent velocity scale. Boundary-Layer Meteorol. 21, 423–441.